JOURNAL OF GEOPHYSICAL RESEARCH, VOL. 115, D05302, doi:10.1029/2009JD013351, 2010

Indirect validation of tropospheric nitrogen dioxide retrieved from the OMI satellite instrument: Insight into the seasonal variation of nitrogen oxides at northern midlatitudes

L. N. Lamsal,[1] R. V. Martin,[1,2] A. van Donkelaar,[1] E. A. Celarier,[3] E. J. Bucsela,[4] K. F. Boersma,[5] R. Dirksen,[5] C. Luo,[6] and Y. Wang[6]

Received 7 October 2009; accepted 26 October 2009; published 6 March 2010.

[1] We examine the seasonal variation in lower tropospheric nitrogen oxides (NO_x = NO + NO_2) at northern midlatitudes by evaluating tropospheric NO_2 columns observed from the Ozone Monitoring Instrument (OMI) satellite instrument with surface NO_2 measurements (SouthEastern Aerosol Research and Characterization and Air Quality System) and current bottom-up NO_x emission inventories, using a global model of tropospheric chemistry (GEOS-Chem). The standard (SP) and DOMINO (DP) tropospheric NO_2 column products from OMI exhibit broadly similar spatial and seasonal variation, but differ substantially over continental source regions. A comparison of the two OMI tropospheric NO_2 products with in situ surface NO_2 concentrations and bottom-up NO_x emissions over the southeast United States indicates that annual mean NO_2 columns from the DP are biased high by 21%–33% and those from the SP are biased high by 27%–43%. The bias in SP columns is highly seasonal, 67%–74% in summer compared with −6% to −1% in winter. Similar seasonal differences exist between top-down and bottom-up NO_x emission inventories over North America, Europe, and East Asia. The air mass factor largely explains the observed seasonal difference between the DP and SP, and in turn the seasonal SP bias. We develop a third product (DP_GC) using averaging kernel information from the DP and NO_2 vertical profiles from GEOS-Chem. This product reduces to 5%–21% the annual mean bias over the southeast United States. We use the seasonal variation in the DP_GC to estimate the seasonal variation in the lifetime of lower tropospheric NO_x against oxidation to HNO_3 over the eastern United States. The effective NO_x lifetime at OMI overpass time (early afternoon) ranges from 7.6 h in summer to 17.8 h in winter, consistent within 3 h of the simulated lifetime. GEOS-Chem calculations reveal that the seasonal variation in OMI NO_2 columns largely reflects gas-phase oxidation of NO_2 in summer with an increasing role for heterogenous chemistry in winter.

Citation: Lamsal, L. N., R. V. Martin, A. van Donkelaar, E. A. Celarier, E. J. Bucsela, K. F. Boersma, R. Dirksen, C. Luo, and Y. Wang (2010), Indirect validation of tropospheric nitrogen dioxide retrieved from the OMI satellite instrument: Insight into the seasonal variation of nitrogen oxides at northern midlatitudes, *J. Geophys. Res.*, *115*, D05302, doi:10.1029/2009JD013351.

1. Introduction

[2] Nitrogen oxides (NO_x = NO + NO_2) are key actors in air quality and climate change. NO_x largely controls the production of tropospheric ozone, forms aerosol nitrate, and affects the abundance of the hydroxyl radical (OH). Nitrogen dioxide (NO_2) is an indicator of surface air quality that is associated with mortality [*Steib et al.*, 2003; *Burnett et al.*, 2004; *Samoli et al.*, 2006] and respiratory morbidity [*Environmental Protection Agency* (*EPA*), 2008]. The U.S. Environmental Protection Agency (EPA) has recently proposed to strengthen the primary NO_2 national air quality standard [*EPA*, 2009]. Major sources of NO_x are combustion, soils, and lightning. Gas-phase formations of HNO_3 during daytime and N_2O_5-hydrolysis during nighttime are the dominant sinks of tropospheric NO_x [*Dentener and Crutzen*, 1993; *Jacob*, 2000]. NO_x observations over broad spatial regions contain information needed to understand NO_x sources and sinks.

[3] Tropospheric NO_2 columns retrieved from satellite measurements have been used to evaluate chemical transport models [*Velders et al.*, 2001; *Martin et al.*, 2002; *Lauer et al.*, 2002; *van Noije et al.*, 2006], to examine spatial and

[1]Department of Physics and Atmospheric Science, Dalhousie University, Halifax, Nova Scotia, Canada.
[2]Also at Harvard-Smithsonian Center for Astrophysics, Cambridge, Massachusetts, USA.
[3]Goddard Earth Sciences and Technology Center, University of Maryland Baltimore County, Baltimore, Maryland, USA.
[4]SRI International, Menlo Park, California, USA.
[5]Climate Observations Department, Royal Netherlands Meteorological Institute, De Bilt, Netherlands.
[6]School of Earth and Atmospheric Sciences, Georgia Institute of Technology, Atlanta, Georgia, USA.

0148-0227/10/2009JD013351$09.00

temporal patterns of NO_x emissions [*Leue et al.*, 2001; *Beirle et al.*, 2003; *Richter et al.*, 2004, 2005; *van der A et al.*, 2006; *Zhang et al.*, 2007; *Boersma et al.*, 2008a; *Kaynak et al.*, 2008], to provide top-down estimates of surface NO_x emissions via inverse modeling [*Martin et al.*, 2003a, 2006; *Müller and Stavrakou*, 2005; *Zhang et al.*, 2007; *Sauvage et al.*, 2007; *Napelenok et al.*, 2008], to examine specific sources [*Jaeglé et al.*, 2004, 2005; *Boersma et al.*, 2005; *Choi et al.*, 2005; *Martin et al.*, 2007; *van der A et al.*, 2008; *Zhao and Wang*, 2009], to infer NO_x lifetimes [*Schaub et al.*, 2007], and to estimate surface NO_2 concentrations [*Lamsal et al.*, 2008]. These analyses, however, are affected by large discrepancies among contemporary tropospheric NO_2 retrievals [*van Noije et al.*, 2006; *Bucsela et al.*, 2008; *Boersma et al.*, 2008a]. Assessments of retrieval quality using independent correlative measurements in a range of environments over all seasons are important for confidence in the accuracy and reliability of these analyses.

[4] Tropospheric NO_2 column retrievals from satellites have been evaluated with in situ NO_2 profile measurements from aircraft [*Heland et al.*, 2002; *Martin et al.*, 2004, 2006; *Boersma et al.*, 2008b; *Bucsela et al.*, 2008; *Celarier et al.*, 2008] and NO_2 column measurements from ground-based instruments [*Lambert et al.*, 2004; *Ionov et al.*, 2008; *Celarier et al.*, 2008; *Brinksma et al.*, 2008; *Kramer et al.*, 2008; *Irie et al.*, 2008; *Wenig et al.*, 2008]. Aircraft offer precise in situ measurements, but these campaign-based validation exercises are limited by sparse spatial and temporal sampling and by the need to extrapolate below the lowest measurement altitude [e.g., *Bucsela et al.*, 2008]. Ground-based tropospheric NO_2 measurements from other novel techniques are yet to be thoroughly evaluated [*Celarier et al.*, 2008]. Validation with in situ surface NO_2 measurements from dense networks of commercial molybdenum converter analyzers are complicated by interference in surface data [*Winer et al.*, 1974; *EPA*, 1975; *Grosjean and Harrison*, 1985; *Fehsenfeld et al.*, 1990; *Ordóñez et al.*, 2006; *Blond et al.*, 2007; *Dunlea et al.*, 2007; *Steinbacher et al.*, 2007; *Lamsal et al.*, 2008]. Observations of "true" NO_2 from photolytic converter analyzers [*Ryerson et al.*, 2000] offer an excellent opportunity to evaluate satellite retrievals. Collocated simultaneous photolytic and molybdenum measurements are valuable for quantifying the interference in molybdenum converter measurements.

[5] Bottom-up NO_x emission inventories from some sources and regions remain quite uncertain, but elsewhere can provide a considerable level of knowledge through aggregation of information from diverse sources. In Canada and the United States, emission inventories provide quantitative estimates of emissions at national, state or provincial, and county levels for many source categories with medium to high level of confidence [*NARSTO*, 2005]. Western European emissions data compiled at the national level annually provide bottom-up emissions with uncertainties of 8%–23% [*Vestreng et al.*, 2009]. The percent uncertainty in total continental emissions is lower than that for individual locations. The use of emission data for indirect validation benefits from a large domain coincident with satellite observations for a variety observational conditions.

[6] Direct observation of the area-averaged NO_x lifetime is difficult. Several previous estimates of the NO_x lifetime are based on in situ observations in industrial and urban plumes [e.g., *Spicer*, 1982; *Dommen et al.*, 1999; *Nunnermacker et al.*, 2000; *Ryerson et al.*, 2003]. Surface NO_x emission inventories over northern midlatitudes exhibit little seasonal variation [*Olivier et al.*, 2001]. Thus, the seasonal variation in tropospheric NO_2 columns provides information on the NO_x lifetime [*Schaub et al.*, 2007]. Retrieval errors must be minimized to reduce errors in the inferred lifetime.

[7] In this paper, we use in situ surface NO_2 measurements and current NO_x emission inventories for indirect validation of satellite retrievals and then go on to estimate the NO_x lifetime. Section 3 compares surface NO_2 concentrations inferred from the Ozone Monitoring Instrument (OMI) satellite instrument with in situ observations from photolytic and molybdenum converter analyzers. In section 4, top-down NO_x emissions inferred from OMI observations are compared with bottom-up emissions over surface sites to understand the magnitude and temporal variation in satellite retrievals. The comparison of top-down and bottom-up emissions is extended to the entire domain of North America (Canada and the United States), Organisation for Economic Co-operation and Development (OECD) Europe, and East Asia. Differences between OMI NO_2 retrievals are examined in section 5. We then apply the OMI NO_2 data to estimate the NO_x lifetime in section 6.

2. Observational Data

2.1. OMI Tropospheric NO_2 Column Retrievals

[8] The OMI aboard the Aura satellite provides measurements of solar backscatter that can be applied to retrieve tropospheric NO_2 with a spatial resolution of up to 13 × 24 km [*Levelt et al.*, 2006b, 2006a]. Aura was launched on 15 July 2004 into a Sun-synchronous polar orbit with a local equator crossing time of 13:45 in the ascending node.

[9] Two independent tropospheric NO_2 column data products from OMI observations are available. These are the OMI standard product (SP; version 1.0.5, collection 3) available from the NASA Goddard Earth Sciences (GES) Data Active Archive Center (http://disc.sci.gsfc.nasa.gov/data/datapool/OMI/) and the DOMINO product (DP) (version 1.0.2, collection 3) available from Tropospheric Emission Monitoring Internet Service (TEMIS) (http://www.temis.nl/). Both algorithms begin with the same slant columns, determined by nonlinear least squares fitting of modeled spectrum to the OMI-measured attenuation spectrum in 405–465 nm window. The slant column represents the integrated abundance of NO_2 along the average photon path from the Sun, through the atmosphere, to the satellite. The two retrieval algorithms differ in the subsequent steps of tropospheric NO_2 column retrieval. Below, we briefly describe the two algorithms for collection 3, which include updates from *Bucsela et al.* [2006] and *Boersma et al.* [2007].

[10] The algorithm for the standard OMI NO_2 data product is described by *Bucsela et al.* [2006, 2008] and *Celarier et al.* [2008]. A 24 h history of slant column densities is used to correct for a cross-track anomaly in the level 1b irradiance measurements as reported by *Dobber et al.* [2008]. The stratospheric (background) NO_2 field is determined by applying masks over regions where tropospheric NO_2 column

abundances are high, smoothing in the meridional direction with a boxcar function, and conducting a zonal planetary wave analysis up to wave 2. The tropospheric air mass factors (AMFs) needed to convert the tropospheric slant columns into vertical columns are computed with the TOMRAD radiative transfer model [*Bucsela et al.*, 2006] using a geographically gridded set of annual mean tropospheric NO_2 vertical profiles for late morning (09:00–12:00 local time) obtained from a GEOS-Chem simulation [*Martin et al.*, 2003b], surface reflectivity from Global Ozone Monitoring Experiment (GOME) [*Koelemeijer et al.*, 2003], and cloud parameters from the OMI O_2–O_2 cloud algorithm [*Acarreta et al.*, 2004]. For cloudy scenes, the below-cloud amount is derived by scaling the NO_2 profile to the retrieved tropospheric NO_2 column. The tropospheric NO_2 columns used in this study typically are about 5% higher than the "polluted" NO_2 columns over northern midlatitude continents.

[11] The DOMINO algorithm [*Boersma et al.*, 2007] begins with the same NO_2 slant column densities processed for the standard product. Stratospheric NO_2 is derived by assimilating OMI NO_2 slant columns into a global chemistry and transport model, TM4 [*Dentener et al.*, 2003]. The tropospheric AMFs are computed as a function of the NO_2 vertical profile simulated by TM4 for the day and time of measurement and the vertically resolved sensitivity to NO_2 of the solar radiation backscattered to space (averaging kernels; *Eskes and Boersma* [2003]) determined with the DAK radiative transfer model [*Stammes*, 2001]. The forward model parameters include cloud parameters based on the cloud model of [*Acarreta et al.*, 2004], surface reflectivity from the TOMS and GOME measurements [*Herman and Celarier*, 1997; *Koelemeijer et al.*, 2003], and viewing geometry.

[12] The retrieved tropospheric NO_2 column is sensitive to the NO_2 profile shape (X_k) used in the calculation of the tropospheric AMFs. *Hains et al.* [2010] evaluated the NO_2 profile from the TM4 model used in the DP and found evidence that the NO_2 profiles in the TM4 model are insufficiently mixed throughout the boundary layer as a result of an implementation error in sampling the NO_2 fields [*Huijnen et al.*, 2009]. NO_2 mixing ratios are more vertically uniform in the unstable mixed layer in GEOS-Chem than in TM4. The DP makes available averaging kernels (A_k) at each level k, which depend only on forward model parameters, when multiplied with the TM4-derived AMF (M) [*Eskes and Boersma*, 2003]. Following the recommendations of *Eskes and Boersma* [2003] and *Boersma et al.* [2004], we combine the DP A_k with the NO_2 profile shapes (X_k^{GC}) from a GEOS-Chem simulation described in Appendix A to remove the influence of TM4 (except for the temperature dependence of the NO_2 cross section). This yields a third data set, DP_GC, which is calculated from each tropospheric slant column density (Ω_s) and an AMF that depends on GEOS-Chem NO_2 profiles:

$$DP\_GC = \frac{\Omega_s \sum_k X_k^{GC}}{M \sum_k A_k X_k^{GC}}. \quad (1)$$

[13] The use of DP_GC allows for a more consistent interpretation with GEOS-Chem. We correct in DP_GC for the cross-track bias in tropospheric slant column densities. The bias was determined for each orbit using NO_2 slant column densities in the 5th to 95th percentile limits over less polluted areas (30°S–5°N) following the approach described by *Celarier et al.* [2008]. Correction of the cross-track bias decreases by ~5% the mean tropospheric NO_2 columns. The stratosphere-troposphere separation in DP_GC remains unchanged from that for DP.

[14] The total error in the retrieval of tropospheric NO_2 columns arises from errors in the slant column density, in the stratosphere-troposphere separation and from the AMF calculation. The uncertainty due to spectral fitting is 0.75×10^{15} molec cm^{-2} [*Boersma et al.*, 2007] and dominates the overall retrieval error over the oceans and remote areas. The uncertainty in the stratospheric slant column density is 0.15×10^{15} molec cm^{-2} for the DP [*Boersma et al.*, 2007] and 0.20×10^{15} molec cm^{-2} for the SP [*Bucsela et al.*, 2006]. AMF errors that arise from the incorrect assumptions on the surface reflectivity, aerosol, clouds, and NO_2 profile shape dominate overall retrieval error over continental source regions [*Martin et al.*, 2002; *Boersma et al.*, 2004, 2007; *Wenig et al.*, 2008]. The estimated errors in the tropospheric NO_2 columns under clear-sky and cloudy conditions are ~30% and ~60%, respectively [*Boersma et al.*, 2004]. The stripe removal may introduce additional bias [*Celarier et al.*, 2008]. We exclude scenes with cloud radiance fraction [*Boersma et al.*, 2004] exceeding 0.5 to reduce the retrieval errors. To reduce spatial averaging, we exclude the ground pixels at swath edges that correspond to a pixel size of more than 50×24 km^2.

2.2. Comparison of OMI NO_2 Retrievals

[15] Here, we compare OMI tropospheric NO_2 columns retrieved from the SP and DP algorithms. Figure 1 shows the seasonal area weighted average tropospheric NO_2 columns gridded to $0.1° \times 0.1°$ from the SP (first row), DP (second row), and DP_GC (third row) over North America for the year 2005. The three products exhibit similarities in their spatial distribution, with pronounced enhancements over major industrial and metropolitan areas. They have a broadly similar seasonal variation, with lower NO_2 columns over industrial source regions in summer than those in winter. Annual mean tropospheric NO_2 columns among the retrievals are well correlated ($r^2 > 0.95$, $N = 216, 651$).

[16] The fourth row of Figure 1 shows the seasonal difference between the DP and SP tropospheric NO_2 columns. Significant differences of more than 5×10^{15} molec cm^{-2} are found over continental source regions. A clear seasonal difference is apparent. Over the domain of North America, the mean tropospheric NO_2 columns in the DP are 42% higher than those for the SP in winter and 22% lower in summer. Seasonal differences between DP and DP_GC (bottom row) are typically within $\pm 1 \times 10^{15}$ molec cm^{-2}. Similar seasonal differences are found for 2006.

2.3. In Situ Surface NO_2

[17] We attempt to understand these differences using hourly in situ measurements of NO_2 from two sources: The SouthEastern Aerosol Research and Characterization (SEARCH) network [*Hansen et al.*, 2003] and the U.S. EPA's Air Quality System (AQS) network [*Demerjian*, 2000]. There are a few complications in comparing satellite

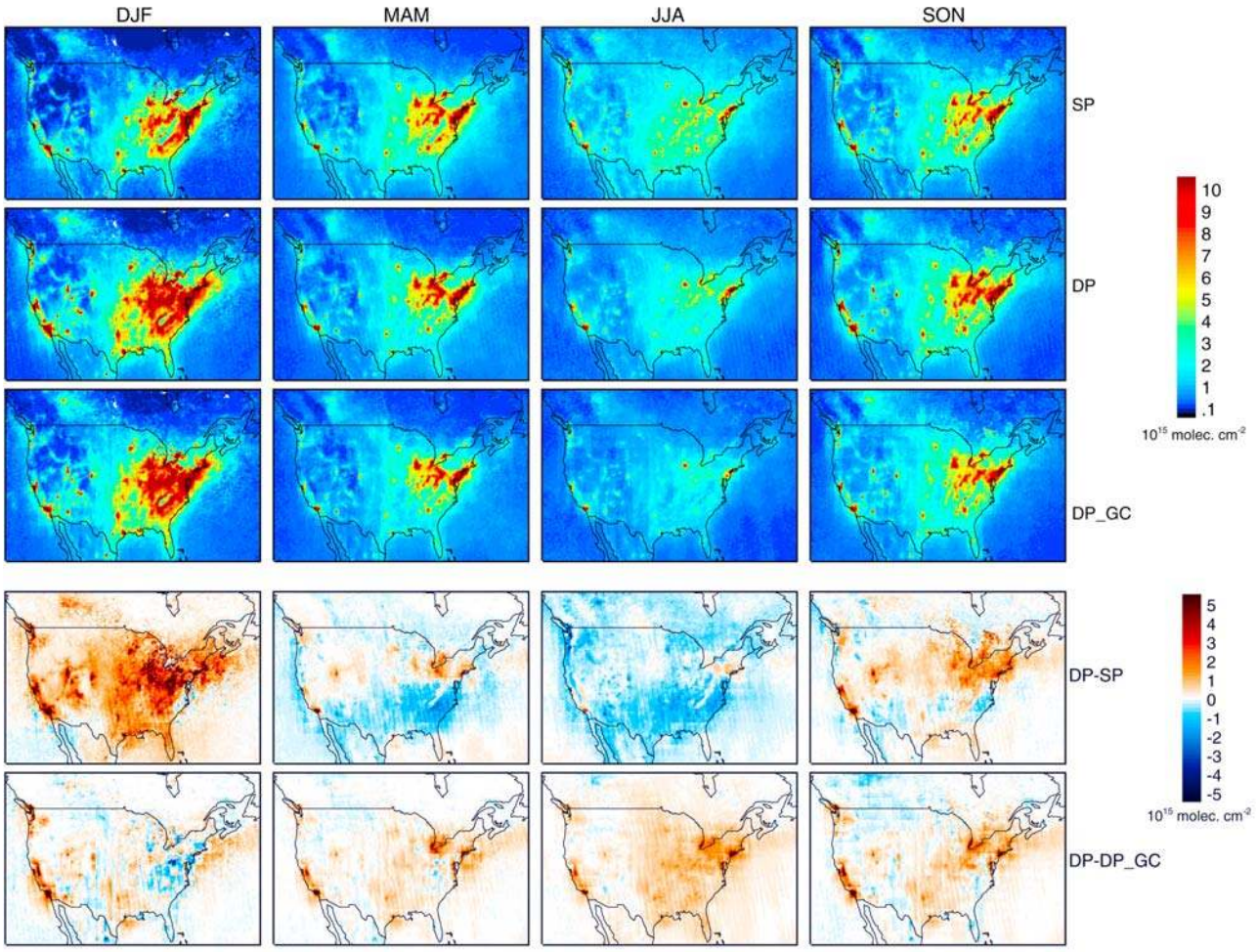

Figure 1. Seasonal mean tropospheric NO_2 columns binned at 0.1° × 0.1° for December–February (DJF), March–May (MAM), June–August (JJA), and September–November (SON) over North America (25°N–55°N, 55°W–130°W) for 2005 from the OMI standard product, SP, (first row), DOMINO product, DP (second row), and a data set based on the DP but using NO_2 profile shapes from the GEOS-Chem model, DP_GC (third row). The bottom rows show the difference between DP minus SP and DP minus DP_GC tropospheric NO_2 columns.

observations with ground-based measurements. Satellite data represent observations that are averaged over a large field of view, covering several hundred square kilometers unlike local point measurements by ground-based instruments. Spatial inhomogeneity within a satellite ground pixel with larger NO_2 concentrations at/near source regions often makes the measurements from a surface site non-representative [*Brinksma et al.*, 2008]. To this end, we focus on the measurements in rural areas. Figure 2 shows the location of the rural stations. Mean tropospheric NO_2 columns over these stations range over 2–6 × 10^{15} molec cm^{-2}, well above the detection limit of the satellite measurements.

[18] NO_2 measurements at SEARCH sites are made using photolytic converter analyzers, a technique that employs broadband photolysis of ambient NO_2 followed by chemiluminescence detection of the product NO [*Kley and McFarland*, 1980; *Ryerson et al.*, 2000]. This method uses wavelength filters to prevent the photolysis of other nitrogen-containing species and therefore offers almost interference-free NO_2 measurements. The potential interferants, HONO

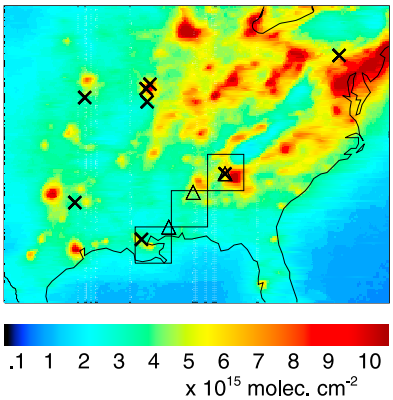

Figure 2. Mean tropospheric NO_2 column over the United States from the OMI SP averaged over the period 2005–2006. Symbols show the location of rural SEARCH (triangles) and EPA/AQS (crosses) sites. The boxes show the GEOS-Chem 2° × 2.5° horizontal grid representing the SEARCH domain.

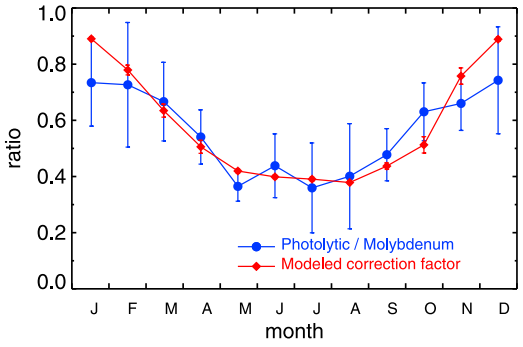

Figure 3. Monthly variation of interference in molybdenum converter measurements at the YRK site in the southeastern United States during 13:00–14:00 local time. The blue line represents the ratio of measurements using the analyzer equipped with the photolytic and molybdenum converters. The red line shows the correction term calculated from a GEOS-Chem simulation. Vertical lines represent the standard deviation of the average divided by the $\sqrt{n}$. Low values of this ratio mean high interference in molybdenum converter measurements.

and NO_3, have very low atmospheric concentrations during the day [*Parrish et al.*, 1990; *Ryerson et al.*, 2000]. Overall uncertainties for 1 h averages in NO_2 are estimated to be ±10% [*Zellweger et al.*, 2000]. Here, we focus on three regionally representative sites: Oak Grove (OAK) in the state of Mississippi, Centreville (CTR) in Alabama, and Yorkville (YRK) in Georgia. The data from these stations are available for 1997–2006.

[19] The NO_2 measurement method of the EPA/AQS network relies on conversion of NO_2 to NO using a heated molybdenum catalytic converter followed by measurement of the resultant NO by chemiluminescence with ozone [*EPA*, 1975]. The molybdenum converter instrument responds not only to NO_2 but also to other reactive nitrogen species [*Winer et al.*, 1974; *EPA*, 1975; *Grosjean and Harrison*, 1985; *Demerjian*, 2000]. The in situ NO_2 concentrations can be overestimated by more than 50% [*Dunlea et al.*, 2007; *Steinbacher et al.*, 2007; *Lamsal et al.*, 2008]. Laboratory studies show that alkyl nitrates and peroxyacetyl nitrate (PAN) are converted to NO with efficiency greater than 92% [*Winer et al.*, 1974; *Grosjean and Harrison*, 1985]. Interference from HNO_3 is difficult to estimate as it can deposit to and evaporate from the surfaces in the inlet manifold [*Neuman et al.*, 1999; *Dunlea et al.*, 2007]. On the basis of measurements at a Swiss site, *Lamsal et al.* [2008] estimated an effective conversion efficiency of ~35% for HNO_3 at OMI overpass time. Here, we use simultaneous measurements of surface NO_2 using molybdenum and photolytic converter analyzers at YRK to test the conversion efficiency of the molybdenum converter.

[20] Figure 3 compares the hourly average surface NO_2 measured by the two instruments during 13:00–14:00 local time over the period 1997–2006. The ratio of photolytic to molybdenum converter measurements, the blue line, gives the relative contribution of interfering species to the molybdenum converter measurements. The observed seasonal variation in the correction factor reflects the seasonal change in the relative contribution of HNO_3, PAN, and other organic nitrates to total reactive nitrogen species, with the largest contribution in summer. The red line indicates the monthly correction factor for 13:00–14:00 local time calculated from the GEOS-Chem simulation following the approach described by *Lamsal et al.* [2008], but assuming a 15% conversion efficiency for HNO_3. The GEOS-Chem-derived seasonal correction factors agree with measurements within 3% for all seasons except in winter, when the modeled correction factor is 16% higher than the measurements. Assuming an HNO_3 conversion efficiency of 35% improves the agreement in winter, but worsens the agreement in other seasons by 12%–17%. The correction factor for urban sites is closer to unity than the rural correction factors found here [*Boersma et al.*, 2009]. We use local GEOS-Chem-derived correction factor to correct for the interference in the molybdenum converter measurements.

3. Comparison of In Situ Measurements With OMI-Derived Surface NO_2

[21] Here we conduct an indirect validation of cloud-free (cloud radiance fraction <0.5) OMI tropospheric NO_2 columns by comparison with coincident ground-based in situ NO_2 measured at 13:00–14:00.

3.1. Inferring Ground-Level NO_2 Concentrations From OMI

[22] We estimate ground-level NO_2 concentrations from OMI for comparison with the in situ measurements. We follow the approach of *Lamsal et al.* [2008] that combines information on the simulated NO_2 vertical profile with information from the satellite observations about the spatial variation of NO_2 concentrations in the boundary layer. Local NO_2 profiles coincident with the OMI observations are taken from the GEOS-Chem simulation.

[23] The ground-level NO_2 mixing ratio S is inferred from OMI tropospheric NO_2 columns Ω as follows:

$$S = \frac{\nu S_G}{\nu \Omega_G - (\nu - 1)\Omega_G^F} \times \Omega, \qquad (2)$$

[24] The subscript "G" denotes GEOS-Chem. The symbol ν represents the ratio of the local satellite NO_2 column to the mean satellite NO_2 column field over a GEOS-Chem grid. The simulated free-tropospheric NO_2 column Ω_G^F is taken as horizontally invariant over a GEOS-Chem grid, reflecting the longer NO_x lifetime in the free troposphere. The satellite-derived surface NO_2 represents the mixing ratio at the lowest vertical layer (100 m) of the model.

[25] Equation (2) implicitly assumes that the tropospheric NO_2 column is dominated by the boundary layer concentrations. This assumption results in a spatial scalar less than ν over regions where the boundary layer concentration is a small fraction of the tropospheric column, yielding the advantage of damping noise in NO_2 columns over regions where there is little NO_2.

3.2. Comparison With Photolytic Converter Measurements

[26] We compare the OMI-derived ground-level NO_2 concentrations with the photolytic converter measurements at three rural sites CTR, OAK, and YRK for 2005–2006.

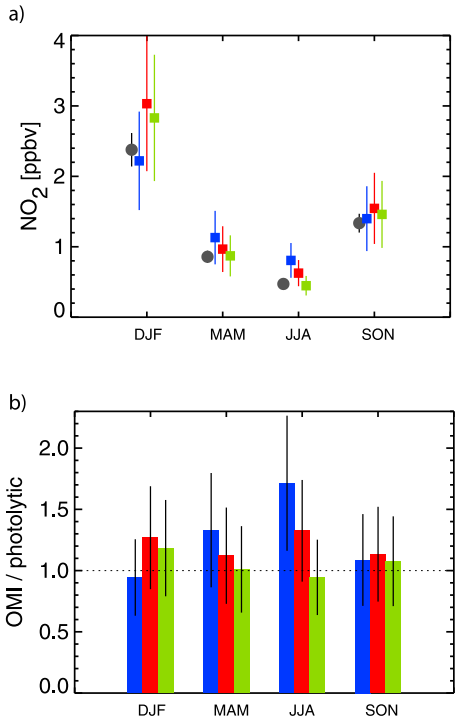

Figure 4. Seasonal variation of NO_2 mixing ratios at rural SEARCH sites for 2005–2006. (a) Seasonal mean NO_2 mixing ratios from photolytic converter measurements (filled circles), and those derived from the OMI SP (blue), DP (red), and DP_GC (green) tropospheric NO_2 columns. In situ data are averaged over 13:00–14:00 local time. Error bars represent errors in photolytic measurements, OMI retrievals, and the GEOS-Chem NO_2 profiles. (b) Seasonal mean ratio of satellite-derived surface NO_2 concentrations from the SP (blue), DP (red), and DP_GC (green) to the in situ surface measurements.

[27] Figure 4a presents the seasonal mean NO_2 mixing ratio from in situ measurements and those derived from the OMI data. The seasonal variation of the OMI-derived NO_2 mixing ratios is broadly consistent with the in situ measurements. However, the amplitude of the seasonal cycles differ. The seasonal mean NO_2 concentrations for the in situ measurements decrease by a factor of 5.1 from the winter (maximum) to the summer (minimum), compared with factors of 2.7 for the SP, 4.8 for the DP, and 6.3 for the DP_GC.

[28] Figure 4b shows the seasonal ratio of the OMI-derived to in situ NO_2 concentration. Values are shown in Table 1. The annual mean bias is 27% for SP, 21% for DP, and 5.3% for DP_GC. The ratio exhibits a strong seasonal variation for the OMI SP with a seasonal bias of 71% in summer and −5.6% in winter. The seasonal variations of the DP-derived and DP_GC-derived surface NO_2 are more consistent with the in situ measurements. With the exception of summer, these results for OMI NO_2 are consistent with the conclusions from earlier comparison of OMI tropospheric NO_2 columns with ground-based and aircraft observations which indicate a bias of −30% to +40% in OMI retrievals [*Boersma et al.*, 2008b; *Brinksma et al.*, 2008; *Bucsela et al.*, 2008; *Celarier et al.*, 2008; *Irie et al.*, 2008; *Lamsal et al.*, 2008].

3.3. Comparison With Molybdenum Converter Measurements

[29] Here, the satellite-derived surface NO_2 concentrations are compared with the corrected molybdenum converter measurements at 8 rural sites over the United States for the years 2005–2006.

[30] Figure 5a shows the OMI-derived seasonal mean NO_2 mixing ratios and those observed from the molybdenum converter instruments. The seasonal cycles of both the satellite-derived and in situ NO_2 concentrations exhibit a winter maximum and summer minimum, similar to those over the SEARCH sites, providing confidence in the corrected data from molybdenum converter. However, the magnitude of the seasonal cycle again differs for the satellite products.

[31] Figure 5b shows the seasonal average ratio of the OMI-derived surface NO_2 and the corrected in situ measurements. Values are given in Table 1. The seasonal mean biases range from −4.5% in winter to 67% in summer for the SP, from 13% in spring to 43% in fall for the DP, and from −5% in summer to 30% in fall for the DP_GC. These seasonal biases are generally consistent with the comparison at the SEARCH sites, recognizing that differences with the SEARCH sites in part reflect different regions of comparison.

4. Seasonal Comparison Between Bottom-Up and Top-Down Emissions

[32] We describe the approach to estimate NO_x emissions from OMI tropospheric NO_2 columns in section 4.2. The seasonal OMI-based top-down estimates are compared with seasonal bottom-up emission inventories in section 4.3.

4.1. Bottom-Up NO_x Emissions Inventory

[33] Table 2 and Figure 6 show the annual and seasonal mean, respectively, of NO_x sources for North America, OECD Europe, and East Asia for the years 2005 and 2006 as implemented in the GEOS-Chem model (Appendix A).

Table 1. Mean Bias in OMI Tropospheric NO_2 Columns Over the Southeast United States Estimated Using In Situ Observations and Bottom-Up Emissions Inventory[a]

	SP			DP			DP_GC		
	Annual	JJA	DJF	Annual	JJA	DJF	Annual	JJA	DJF
Photolytic in situ	27	71	−5.6	21	33	27	5.3	−5.5	18
Corrected molybdenum	28	67	−4.5	33	36	39	14	−5.7	29
Bottom-up emissions	43	74	−1	30	25	33	21	2.9	31

[a]Values indicate the difference in percent.

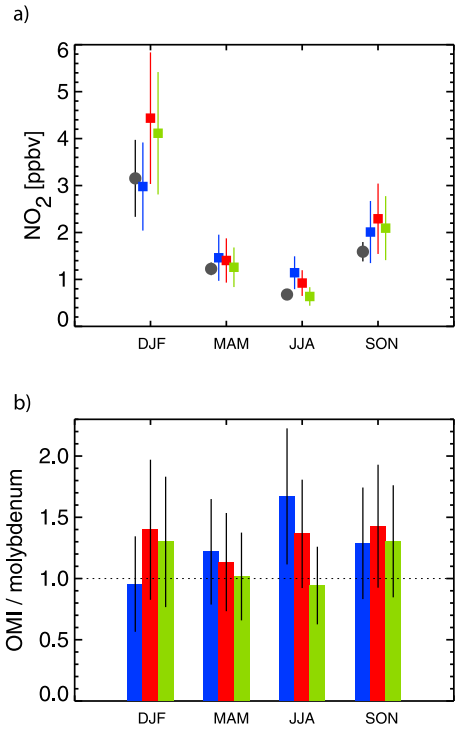

Figure 5. Seasonal variation of NO_2 mixing ratios at rural EPA/AQS sites for 2005–2006. (a) Seasonal mean NO_2 mixing ratios from molybdenum converter measurements (filled circles) and those derived from the OMI SP (blue), DP (red), and DP_GC (green) tropospheric NO_2 columns (squares). In situ data are averaged over 13:00–14:00 local time and are corrected for interference using a GEOS-Chem simulation. Error bars in molybdenum converter measurements are calculated from errors in photolytic converter and the seasonal difference between photolytic and corrected molybdenum converter measurements. Error bars in the OMI-derived surface NO_2 represent errors in retrievals and in the GEOS-Chem NO_2 profiles. (b) Seasonal mean ratio of satellite-derived surface NO_2 concentrations from the SP (blue), DP (red), and DP_GC (green) to the in situ surface measurements.

Table 2. Average GEOS-Chem NO_x Emissions Over North America, OECD Europe, and East Asia for the Years 2005–2006

Source	Emission Rate (Tg N yr^{-1})		
	North America	OECD Europe	East Asia
Fossil fuel combustion	5.29	2.71	7.36
Lightning	0.70	0.09	0.27
Biomass burning	0.15	0.03	0.05
Soils	0.67	0.34	0.57
Biofuels	0.03	0.10	0.01
Aircraft	0.16	0.07	0.02

The bottom-up inventories over these regions incorporate detailed source characterization as well as emission factors representative of country-specific emission rates [*NARSTO*, 2005; *Streets et al.*, 2006; *Zhang et al.*, 2007; *Vestreng et al.*, 2007]. Anthropogenic activities contribute >75% of total NO_x emissions. For North America and OECD-Europe, the anthropogenic NO_x emissions are dominated by on- and off-road engines and vehicles (~55%) followed by electric utilities (~20%), and industrial and residential combustion (~20%). The seasonal variation in area (e.g., on-road/non-road mobile, small industries) sources in the VISTAS emission inventory [*Morris et al.*, 2007] for the United States is <1%. Seasonal controls on power plant emissions drive the summer time reduction in anthropogenic NO_x emissions [*Frost et al.*, 2006; *Hudman et al.*, 2007]. Biogenic and pyrogenic emissions exhibit strong seasonal variation with the maximum emissions occurring in summer, but are a small fraction (<9%) of total surface NO_x emissions.

[34] The overall uncertainty in the seasonal variation in anthropogenic NO_x emissions is expected to be <25% over OECD Europe [*Vestreng et al.*, 2009] and the United States (Christian Hogrefe, personal communication, 2008). The uncertainty in seasonal variation in power plant NO_x emissions in the United States is fairly small due to the use of Continuous Emission Monitoring Systems (CEMS) [*Frost et al.*, 2006]. The overall uncertainty for Asian NO_x emissions is relatively large (±37%) [*Streets et al.*, 2003; *Zhang et al.*, 2007, 2009]. The well-established seasonal variation in NO_x emissions for North America and OECD Europe is a valuable data set for indirect validation of the OMI data.

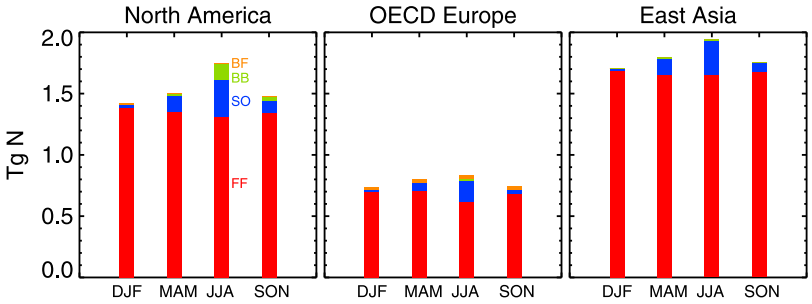

Figure 6. Seasonal NO_x emissions for 2005–2006 from surface sources over land of North America, OECD Europe, and East Asia for various source categories: fossil fuel combustion (FF), soil (SO), biomass burning (BB), and biofuel (BF).

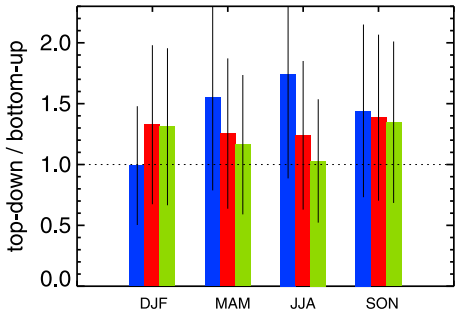

Figure 7. Seasonal mean ratio of top-down surface NO_x emissions to bottom-up emissions averaged over the SEARCH sites (Figure 2) as inferred from the OMI SP (blue bars), DP (red bars), and DP_GC (green bars). Error bars represent uncertainty in bottom-up inventory, in the inversion, and in OMI retrievals.

4.2. Top-Down NO_x Emissions Estimate

[35] We use the mass balance approach [*Leue et al.*, 2001] as described by *Martin et al.* [2003a] to relate OMI tropospheric NO_2 columns (Ω) to surface NO_x emissions (E):

$$E = \frac{E_G}{\Omega_G} \times \Omega. \tag{3}$$

[36] Here, Ω_G is the tropospheric NO_2 column from the GEOS-Chem simulation sampled at satellite overpass time and based on the a priori emissions E_G. We adopt the improvement of *Wang et al.* [2007] to account for contributions from external and free-tropospheric sources such as lightning. These contributions were identified with a sensitivity simulation in which local land surface emissions are turned off and subtracted from both the retrieved and simulated NO_2 columns. We infer daily surface NO_x emissions over coasts and continents. We take the uncertainty in the inversion to be 30% [*Martin et al.*, 2003a]. The use of E_G/Ω_G generally yields an effective NO_x lifetime that accounts for local NO_x chemistry and transport. However, because of spatial smearing [*Palmer et al.*, 2003], the grid average NO_2 column in part reflects nearby NO_x emissions. We considered the approach by *Toenges-Schüller et al.* [2006] and *Boersma et al.* [2008b] to account for the emissions from adjacent grid cells:

$$E_{i,j} = \frac{E_{G_{i,j}}}{\sum_{n=-1}^{1}\sum_{m=-1}^{1} K_{i,j} E_{G_{i+m,j+n}}} \times \frac{E_{G_{i,j}}}{\Omega_{G_{i,j}}} \times \Omega_{i,j}, \tag{4}$$

with the kernel K defined as $\frac{1}{p+8}\begin{bmatrix} 1 & 1 & 1 \\ 1 & p & 1 \\ 1 & 1 & 1 \end{bmatrix}$. The correlation between the smoothed bottom-up emissions and the corresponding GEOS-Chem tropospheric NO_2 columns is maximum with the smoothing parameter $p > 1000$; therefore, application of equation (4) is unnecessary here.

4.3. Comparison

[37] Here we compare the satellite-derived emission estimates with the bottom-up inventories. Given that the inter-retrieval differences exceed the uncertainty in the bottom-up inventories, we interpret here the differences between top-down and bottom-up emissions for insight into retrieval biases. We first focus on the area where the three SEARCH sites are located.

[38] Figure 7 presents the ratio of seasonal total top-down and bottom-up surface NO_x emissions over the SEARCH domain specified in Figure 2. Mean biases are in Table 1. The seasonal mean DP-based emissions are 24%–38% higher and the DP_GC-based emissions are 2.9%–34% higher than the a priori. The seasonal mean SP-based emissions are within 1% of the a priori in winter but 74% higher in summer. The seasonal biases in satellite retrievals inferred from bottom-up surface NO_x emissions and in situ surface measurements (Figure 4) generally agree to within 15%. Similar seasonal discrepancies provide confidence in both methods of indirect validation. Small differences between the two approaches could arise from the different domains, in the observation period, and by seasonal nonlinearity between the surface NO_x emissions and the corresponding NO_2 column [*Kunhikrishnan and Lawrence*, 2004]. We extend the emissions comparison to larger geographic areas over the entire domain of North America, OECD Europe, and East Asia.

[39] Figure 8 shows the spatial variation of regional bottom-up and top-down NO_x inventories of land surface emissions. Both top-down and bottom-up inventories exhibit broad similarity in their spatial pattern. However, pronounced differences in the magnitude of NO_x emissions are observed.

[40] Figure 9 shows the ratio of seasonal area-averaged top-down and bottom-up NO_x emissions over North America, OECD Europe, and East Asia. The ratio ranges from 0.97 to 2.03 for the SP, from 1.32 to 1.66 for the DP, and from 1.10 to 1.49 for the DP_GC. The overall comparison is generally consistent with the conclusions for the Eastern United States (Figures 4–7). For the SP the difference is smallest in winter and largest in summer. The seasonal variation in the DP top-down emissions is similar to the bottom-up. The bias versus the bottom-up is reduced significantly with the top-down estimates based on the DP_GC. We recommend using the DP_GC product for quantitative applications of the OMI NO_2 data.

5. Synthesis of Indirect Validation Across Multiple Methods

[41] Sections 3 and 4 presented consistent results of satellite-derived surface NO_2 versus the surface measurements (Figures 4 and 5, Table 1) and top-down versus bottom-up emission inventories (Figures 7 and 9, Table 1) that together indicate a seasonal bias in the satellite retrievals. Retrievals of tropospheric NO_2 columns are affected by the air mass factor and the removal of the stratosphere. Here we examine the relative contribution of each component to the observed difference between the DP and SP.

[42] We first calculate the difference between the DP and SP tropospheric NO_2 columns that arises from the stratosphere-troposphere separation. The change in the tropospheric vertical column $\Delta\Omega_v^{DP-SP}$ arising from the stratosphere-troposphere separation is the difference in the stratospheric slant columns $\Omega_{s,strat}$ in the two retrievals divided by the tropospheric air

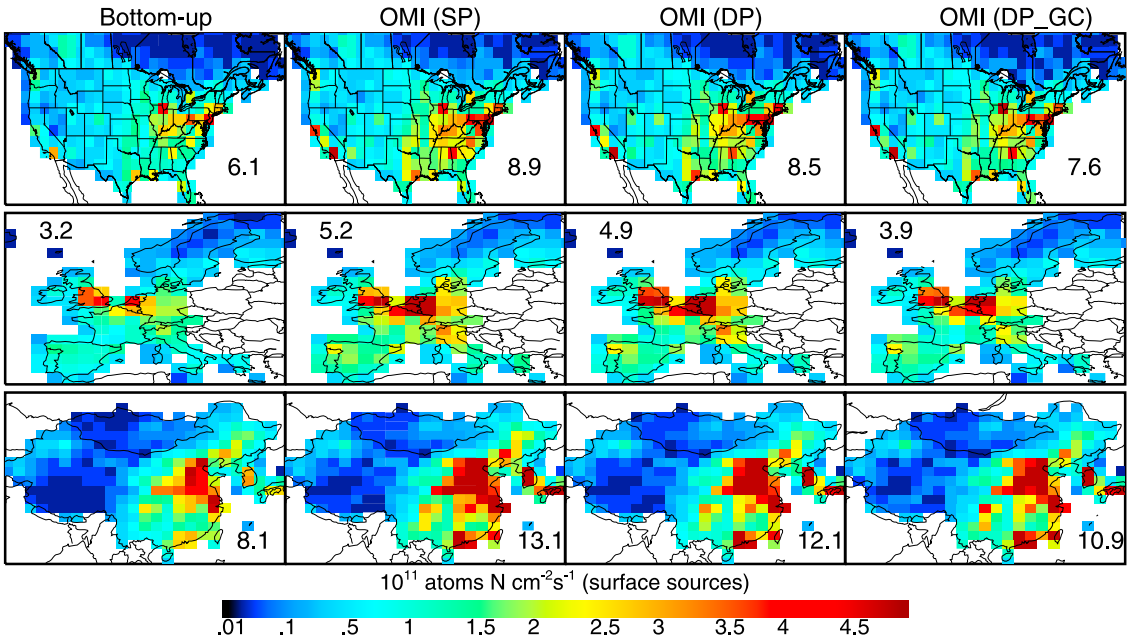

Figure 8. Annual mean surface NO_x emissions over North America (top), OECD-Europe (middle), and East Asia (bottom) for 2005 and 2006. The left column contains bottom-up emissions from fossil fuels, biofuels, biomass burning, and soils. The other columns contain top-down emissions estimated using OMI tropospheric NO_2 columns from the SP, DP, and DP_GC. Numbers in Figure 8 indicate annual mean emissions in Tg N Yr^{-1}.

mass factor M. The SP stratospheric slant columns ($\Omega^{SP}_{s,strat}$) are calculated from the stratospheric NO_2 vertical columns and the SP stratospheric AMFs. We use values of M from only one retrieval algorithm to isolate the effect of the stratosphere:

$$\Delta\Omega^{DP-SP}_{v,strat} = \frac{\Omega^{DP}_{s,strat} - \Omega^{SP}_{s,strat}}{M^{DP}}. \quad (5)$$

[43] Figure 10 (left) shows the seasonal difference between the DP and SP tropospheric NO_2 columns due to their different algorithms for the stratosphere-troposphere separation. The stratospheric NO_2 slant columns in the two products generally agree to within $\pm 1 \times 10^{15}$ molec cm^{-2}. The effect on the troposphere can be larger at northern midlatitudes due to lower air mass factors. The seasonal difference at northern midlatitudes due to the stratosphere-troposphere separation can be opposite in sign to the difference in Figure 1.

[44] The difference between the DP and SP tropospheric vertical NO_2 columns caused by their different AMF can be calculated by applying their respective AMFs to the same tropospheric slant columns:

$$\Delta\Omega^{DP-SP}_{v,AMF} = \frac{\Omega^{SP}_{s,trop}}{M^{DP}} - \frac{\Omega^{SP}_{s,trop}}{M^{SP}} \quad (6)$$

[45] Figure 10 (middle) shows the AMF-induced difference in the tropospheric NO_2 columns. Differences are largest at northern midlatitudes, and smallest over ocean. At northern midlatitudes in winter, spring, and fall DP AMFs are lower than SP AMFs, leading to larger DP tropospheric NO_2 columns. The sign reverses in summer when DP AMFs exceed SP AMFs. The OMI Science Team understands that

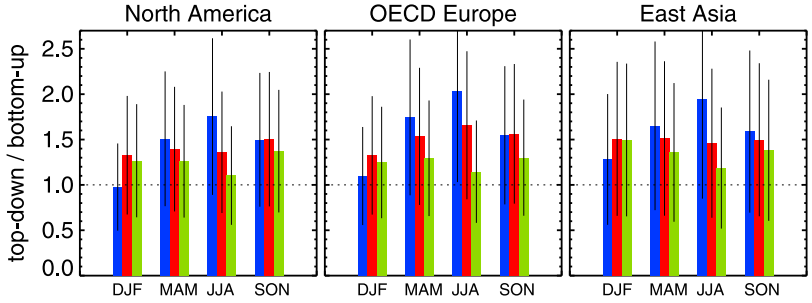

Figure 9. Seasonal mean ratio of area-averaged top-down surface NO_x emissions to bottom-up emissions over (left) North America, (middle) OECD Europe, and (right) East Asia. Error bars represent uncertainty in bottom-up inventories, in the inversion, and in OMI retrievals. Bars are colored as in Figure 7.

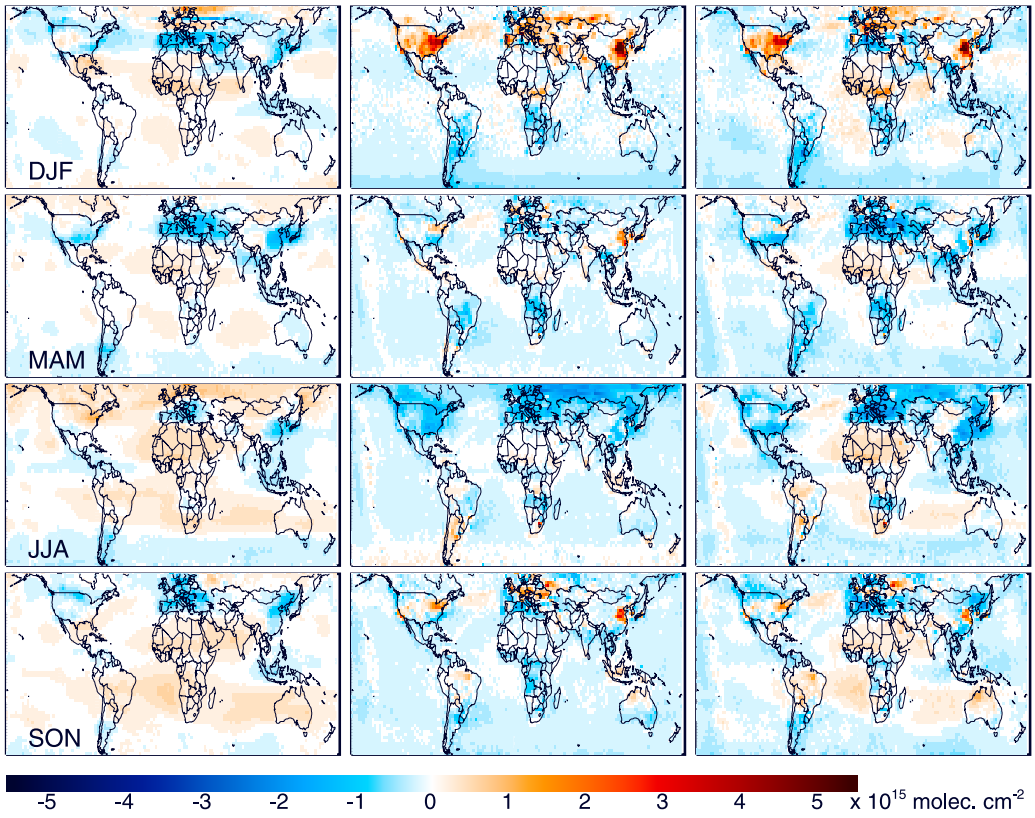

Figure 10. Seasonal difference between the (left) DP minus SP tropospheric NO_2 columns due to the difference in the stratosphere-troposphere separation, (middle) the air mass factor, and (right) their combination.

these differences arise in part from the use of annual mean NO_2 profiles in the SP algorithm. A future SP algorithm is being developed to use monthly varying NO_2 vertical profiles to better account for seasonal variation in free-tropospheric NO_x and in mixed-layer depths. Other sources of AMF differences arise from difference in terrain pressures [e.g., *Zhou et al.*, 2009], radiative transfer algorithms, and surface reflectivity used in the two products. The existing difference in surface reflectivities of >0.02 [*Bucsela et al.*, 2008] between the two algorithms can have significant effect in polluted areas with low reflectivities [*Martin et al.*, 2002; *Boersma et al.*, 2004; *Hains et al.*, 2010].

[46] Figure 10 (right) shows the combined effect of the difference in the stratosphere-troposphere separation and air mass factors to the observed difference between the two products. The effect of the air mass factor is partially compensated by the effect of the stratospheric correction. Consequently, most regions of the world exhibit little change. However, pronounced seasonal differences remain over the industrial regions, with the DP being higher than the SP in winter. The sign and magnitude of the combined differences largely explain the observed seasonal differences between the two products shown in Figure 1.

6. Seasonal Variation in NO_x

[47] In situ and OMI-derived surface NO_2 concentrations exhibit a distinct peak in winter, with a minimum in summer (Figures 4 and 5). Three factors that could drive this seasonal variation are NO_x emissions, the NO/NO_2 ratio, and the NO_x lifetime. Figure 6 shows that the seasonal variation in NO_x emissions does not explain the observed seasonal change in NO_2 concentrations. Seasonal variation in the NO_2/NO_x ratio at SEARCH sites during OMI overpass time is <10%. *Velders et al.* [2001] recognized that the seasonal variation in tropospheric NO_2 columns is driven by the NO_x lifetime. An inspection of the seasonal variation in the tropospheric NO_2 columns, coupled with the weak seasonal variation in emissions, indicates that the NO_x lifetime at northern midlatitudes varies by about a factor of two. *Schaub et al.* [2007] applied SCIAMACHY NO_2 columns to infer the NO_x lifetime over Switzerland, where NO_x emissions are well known. We extend their approach here over the eastern United States.

[48] Tropospheric NO_2 columns observed by OMI at time 't_{OMI}' reflect previous NO_x emissions emitted at time (t_i) that decay exponentially with effective NO_x lifetime τ. We calculate the effective NO_x emissions (E_{eff}) preceding OMI observations as the weighted average with weights ($w_i = \exp[-t_{OMI} - t_i)]/\tau$). This relationship allows inference of τ from OMI observations (Ω):

$$\tau = \beta \times \frac{\Omega}{E_{eff}}, \quad (7)$$

where β is the ratio of tropospheric NO_x to NO_2 columns obtained from the GEOS-Chem model. Because E_{eff} itself depends on τ, we find the solution iteratively. We apply the

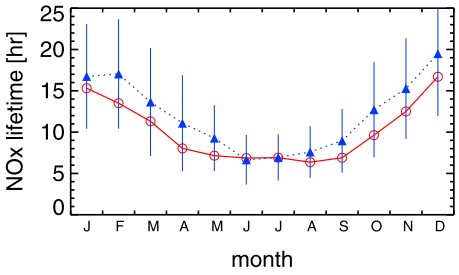

Figure 11. Monthly tropospheric lifetime of NO_x against oxidation to stable reservoirs over the eastern United States for 2005, as calculated from the GEOS-Chem model (red line with circles) and OMI measurements (blue dotted line with triangles). The bars represent the standard deviation of the average.

calculation to the DP_GC product, for which the validation indicated the greatest confidence. As recommended by *Eskes and Boersma* [2003] and *Boersma et al.* [2004], the use of DP_GC also has the benefit of allowing a consistent interpretation since NO_2 profiles used in the retrieval are from the same model used for the interpretation. We limit our calculation to polluted (winter NO_2 columns $>2 \times 10^{15}$ molec cm^{-2}) areas of the eastern United States where the columns are dominated by the lower troposphere.

[49] Figure 11 shows the monthly average lifetime of NO_x at 13:00–14:00 h in the lower troposphere. The lifetime exhibits strong seasonal variation with a maximum in winter and a minimum in summer. The monthly mean effective lifetime ranges 6.7–19.5 h for OMI and 6.4–16.7 h for GEOS-Chem. The seasonal mean lower tropospheric NO_x lifetimes presented here are consistent with the estimates of *Schaub et al.* [2007] over Switzerland from SCIAMACHY and of *Beirle et al.* [2003] over Germany from GOME, with the exception in summer. Previous studies based on measurements in power plant and industrial plumes report a large spatial variability (1.5–6.4 h in summer) [*Spicer*, 1982; *Nunnermacker et al.*, 1998, 2000; *Dommen et al.*, 1999; *Sillman*, 2000; *Ryerson et al.*, 2003]. The in situ based estimates are expected to be lower than the area-averaged NO_x lifetimes derived from OMI because of influence from free tropospheric NO_x on the OMI calculation.

[50] The loss of NO_x mainly occurs through the formation of HNO_3 by the reaction of NO_2 with OH and by aerosol uptake of NO_2, NO_3, and N_2O_5. We examine their relative contribution for insight into the chemical mechanism that controls the seasonal variation of the NO_x lifetime and OMI NO_2 columns. Figure 12 presents the time-averaged fraction of total NO_x loss to HNO_3 contributed by the two chemical mechanisms as simulated with GEOS-Chem. The fraction of HNO_3 formed by gas-phase reaction of NO_2 with OH ranges from 85% (winter) to 99% (summer) during OMI overpass time and from 25% (winter) to 73% (summer) diurnally averaged. The uptake of NO_2, NO_3, and N_2O_5 by aerosols is more effective for nighttime formation of HNO_3 and accounts for <1% during 13:00–14:00 LT and 26% on daily average in summer. The chemistry controlling the effective NO_x lifetime inferred from OMI lies between these two extremes. Both extremes indicate that gas-phase chemistry controls the effective NO_x lifetime in summer. However, in winter the diurnally averaged curve is more appropriate as the effective NO_x lifetime approaches 24 h. The effective NO_x lifetime inferred from OMI in winter reflects a larger influence from heterogeneous chemistry.

7. Conclusion

[51] We examined the seasonal variation of lower tropospheric NO_x at northern midlatitudes using surface NO_2 measurements, bottom-up inventories of surface NO_x emissions, tropospheric NO_2 column retrievals from the OMI satellite instrument, and a global model of tropospheric chemistry (GEOS-Chem). Tropospheric NO_2 columns retrieved from OMI using the standard (SP) and DOMINO (DP) algorithms exhibit similar spatial variation ($r^2 = 0.9$) over North America, but pronounced differences in their seasonal variation.

[52] Tropospheric NO_2 retrievals are sensitive to assumed NO_2 profile shapes. We used averaging kernel information available from the DP to effectively replace the a priori profiles from TM4 by NO_2 profiles from a GEOS-Chem simulation and produce a third data set (DP_GC). NO_2 mixing ratios in the GEOS-Chem simulation are more vertically uniform within the unstable mixed layer, in contrast with NO_2 mixing ratios in the TM4 simulation, which are more sharply peaked near the surface. We applied an improved destriping algorithm to correct for the cross-track bias in the DP_GC.

[53] We indirectly validated OMI tropospheric NO_2 columns with surface NO_2 measurements by applying coincident GEOS-Chem NO_2 profiles as a transfer function. The satellite-derived surface NO_2 was compared with the photolytic (SEARCH) and molybdenum converter (EPA/AQS) measurements at rural sites in the United States. Coincident photolytic and molybdenum converter measurements in the southeast United States (YRK) were used to estimate an effective HNO_3 detection efficiency of 15% for OMI overpass time. NO_2 measurements from molybdenum converter analyzers were corrected for interference using coincident simulated values of HNO_3, PAN, and alkyl nitrates from GEOS-Chem. The seasonal average of the photolytic and

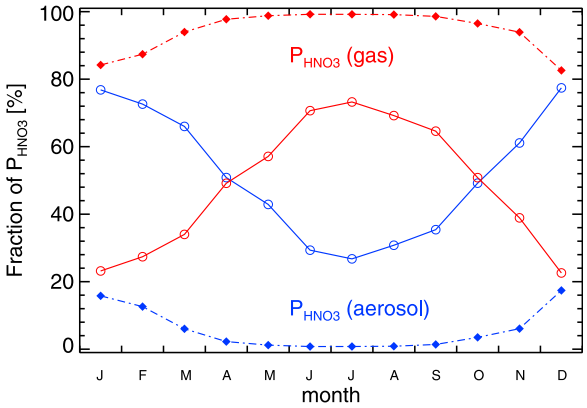

Figure 12. Simulated monthly fraction of total HNO_3 production (NO_x loss) in the boundary layer. Red lines indicate the contribution from reaction of NO_2 with OH (P_{HNO3} (gas)). Blue lines indicate aerosol uptake of NO_2, NO_3, and N_2O_5 (P_{HNO3} (aerosol)). Values are daily (solid line with circles) and 1 h (13:00–14:00 LT, dash-dotted line with diamonds) average results from GEOS-Chem over the eastern United States for 2005.

corrected molybdenum converter measurements agree to within 1%, with the exception in winter. The seasonal variation of the satellite-derived surface NO_2 and surface measurements is broadly consistent, but differs in the seasonal amplitude. The mean seasonal difference between satellite-derived surface NO_2 and photolytic measurements ranges from −5.6% (winter) to 71% (summer) for the SP, from 12% (spring) to 33% (summer) for the DP, and from −5.5% (summer) to 18% (winter) for the DP_GC. A comparison with the corrected molybdenum converter measurements yields consistent seasonal discrepancies.

[54] We indirectly validated the satellite retrievals of tropospheric NO_2 columns with well-established seasonal bottom-up surface NO_x emission inventories for the southeast United States. The bottom-up emissions exhibit little seasonal variation and have an uncertainty of 25% at the regional scale. The GEOS-Chem model was used to infer from OMI NO_2 top-down estimates of NO_x emissions. Over the SEARCH sites, the seasonal mean biases between OMI and bottom-up emissions range from −1% (winter) to 74% (summer) for the SP, from 24% (spring) to 38% (fall) for the DP, and from 2.9% (summer) to 34% for the DP_GC. The larger inter-retrieval difference in top-down emissions than that in bottom-up emissions permits the evaluation of the retrievals rather than bottom-up emissions through this approach. The seasonal biases in top-down emissions are similar to those between in situ and satellite-derived surface NO_2, providing confidence in both indirect validation techniques. We recommend using the DP_GC product for quantitative applications of the OMI NO_2 data.

[55] We extended the comparison between top-down and bottom-up annual mean surface NO_x emissions to North America, OECD Europe, and East Asia. The SP top-down inventory is higher than the bottom-up inventory by 45% over North America and 62% over East Asia and OECD Europe, with the largest difference (75%–100%) in summer. The DP-based emissions are higher than the bottom-up emissions by 39% over North America, 52% over OECD Europe, and 49% over East Asia. The DP_GC-based top-down inventory is 10%–38% higher than the bottom-up inventory over the three regions.

[56] We assessed the contribution of the stratosphere-troposphere separation and air mass factors to the observed difference between the DP and SP tropospheric NO_2 columns. The effect of the different stratospheric NO_2 columns on the tropospheric columns is generally small ($<1 \times 10^{15}$ molec cm^{-2}). However, this difference can dominate in the tropics and over oceans. The contribution of air mass factors is more important over continental source regions where it generally causes a larger seasonal variation in DP than in SP. The lack of seasonal variation in the SP a priori is a key reason for the seasonal differences in air mass factors.

[57] The seasonal variation in OMI NO_2 columns is primarily driven by seasonal variation in the NO_x loss rate at northern midlatitudes, where NO_x emissions exhibit little seasonal variation. We exploited this information to estimate the seasonal NO_x lifetime from OMI NO_2 observations. The resultant monthly average tropospheric NO_x lifetime over the eastern United States is 6.7–19.5 h, in close agreement by 3 h of the lifetime calculated from the GEOS-Chem model. We use the GEOS-Chem model to calculate that the effective NO_x lifetime observed by OMI is driven by the formation of HNO_3 by gas-phase reaction of NO_2 with OH in summer, with an increasing role for heterogenous chemistry in winter. Observation of the seasonal variation in NO_2 from other satellite instruments such as GOME-2 with overpass times earlier in the day will be more strongly influenced by aerosol processes.

[58] The work presented here serves as indirect validation of satellite products. On the basis of this analysis, we recommend switching from annual to monthly NO_2 profiles in the SP algorithm, using a stripe correction in DP, reconsidering the boundary layer mixing scheme used to generate NO_2 profiles, reevaluating the stratosphere-troposphere separation algorithms, moving toward a common surface reflectivity database, and following the example of DP that all solar backscatter trace gas products make averaging kernel (or scattering weight) information available so that profile assumptions can be removed. A higher resolution simulation may better capture sharp horizontal gradients in the a priori NO_2 profile in the boundary layer. Direct validation of satellite observations with in situ and ground-based measurements over wide geographic regions over an extended period of time will be valuable for further understanding of seasonal processes. Replacement of molybdenum converter analyzers with "true" NO_2 capability would better address compliance needs in light of the EPA's proposed NO_2 standard, contribute to air quality research, and facilitate satellite validation.

Appendix A: The GEOS-Chem Model

[59] GEOS-Chem is a global three-dimensional model of tropospheric chemistry driven by assimilated meteorological data available from the Goddard Earth Observing System at the NASA Global Modeling and Assimilation Office (GMAO). The model has recently been applied to interpret a variety of NO_x observations [*Martin et al.*, 2006, 2007; *Hudman et al.*, 2007, 2009; *Sauvage et al.*, 2007; *Boersma et al.*, 2008a, 2009; *Lamsal et al.*, 2008; *Zhang et al.*, 2008]. GEOS-Chem simulations generally agree to within 30% of measured NO_x, HNO_3, and PAN over eastern North America [*Martin et al.*, 2006; *Hudman et al.*, 2007; *Singh et al.*, 2007].

[60] Here we use version 8-01-04 (http://acmg.seas.harvard.edu/geos/) of the model for simulation at 2° × 2.5° using GEOS-4 meteorological fields. The GEOS-4 data have 55 vertical levels between surface and 0.1 hPa and a temporal resolution of 6 h. Data for surface variables and mixing depths are given every 3 h. There are about 16 levels in the troposphere, including five levels below 2 km. The chemical time step in the model is 1 h.

[61] The model includes a detailed simulation of tropospheric ozone-NO_x-hydrocarbon chemistry as well as of aerosols and their precursors. The aerosol and gaseous simulations are coupled through the formation of sulphate and nitrate, the HNO_3/NO_3^- partitioning of total inorganic nitrate, heterogeneous aerosol chemistry including uptake of N_2O_5 by aerosols [*Jacob*, 2000; *Evans and Jacob*, 2005], and aerosol effects on photolysis rates [*Martin et al.*, 2003b].

[62] The global NO_x emission inventory in GEOS-Chem has been recently updated [*van Donkelaar et al.*, 2008]. Canadian emissions are based on the CAC inventory (http://

www.ec.gc.ca/pdb/cac/) for 2005. Mexican emissions are based on BRAVO [*Kuhns et al.*, 2005] for 1999. We update here the fossil fuel NO_x inventory for the United States, OECD Europe, and East Asia. Anthropogenic emissions over the United States are based on the VISTAS inventory (http://www.vistas-sesarm.org) for the year 2002. Diurnal variations are based on the EDGAR inventory [*Olivier et al.*, 2001]. Weekly variation is based on the U.S. EPA National Emissions Inventory for 1999 (http://www.epa.gov/chief/net/1999inventory.html). We scale the VISTAS 2002 emissions to the year of simulation (i.e., 2005 and 2006) according to source- and state-specific emission trends available from the U.S. EPA. The scale factors are monthly and include regulated changes in emissions. We update the European inventory to EMEP for 2005. The East Asian emissions (http://www.cgrer.uiowa.edu/EMISSION_DATA_new/data/intex-b_emissions/) are for the year 2006, with monthly variation based on the work of *Zhang et al.* [2007].

[63] Other NO_x sources are biomass burning, soil, and lightning. Biomass burning emissions are from a climatological inventory with seasonal variability estimated using Along Track Scanning Radiometer (ATSR) fire counts [*Duncan et al.*, 2003]. Diurnal variation in biomass burning emission is based on hourly fire counts over central America detected by the Geostationary Operational Environmental Satellite (GOES-4) for 2002 as described by *Boersma et al.* [2008a]. Soil NO_x emissions are computed as a function of vegetation type, precipitation, temperature, fertilizer usage, and leaf area index [*Yienger and Levy*, 1995; *Wang et al.*, 1998]. All surface emissions are distributed vertically in the unstable mixed layer [*Martin et al.*, 2003b]. Emissions of NO_x from lightning are linked to deep convection following the parameterization of *Price and Rind* [1992] with vertical profiles taken from *Pickering et al.* [1998]. The midlatitude lightning NO_x source is 1.6 Tg N yr^{-1} following *Martin et al.* [2006] and *Hudman et al.* [2007]. The spatial distribution of lightning flashes is scaled to OTD-LIS following *Sauvage et al.* [2007] and L. Murray et al. (manuscript in preparation, 2010). Nitric oxide emissions from aircraft are based on the monthly mean emission inventory compiled by *Baughcum et al.* [1996]. The cross-tropopause NO_y flux calculated from N_2O oxidation in the model stratosphere [*Bey et al.*, 2001] contributes 0.1 Tg N yr^{-1} as NO_x and 0.4 Tg N yr^{-1} as HNO_3.

[64] **Acknowledgments.** We are grateful to Eric S. Edgerton, Ben Hartsell, and Callie Waid for providing the SEARCH data. We thank the OMI, AQS, and TEMIS teams for making the data available. This work was supported by NASA's Atmospheric Composition Program and Canadian Foundation for Climate and Atmospheric Science.

References

Acarreta, J. R., J. F. de Haan, and P. Stammes (2004), Cloud pressure retrieval using the O_2–O_2 absorption band at 477 nm, *J. Geophys. Res.*, *109*, D05204, doi:10.1029/2003JD003915.

Baughcum, S. L., T. G. Tritz, S. C. Henderson, and D. C. Pickett (1996), Scheduled civil aircraft emission inventories for 1992: Database development and analysis, *Tech. Rep.*, Nat. Aeronaut. and Space Admin., Washington, D.C., NASA CR-4700.

Beirle, S., U. Platt, M. Wenig, and T. Wagner (2003), Weekly cycle of NO_2 by GOME measurements: A signature of anthropogenic sources, *Atmos. Chem. Phys.*, *3*, 2225–2232.

Bey, I., et al. (2001), Global modeling of tropospheric chemistry with assimilated meteorology: Model description and evaluation, *J. Geophys. Res.*, *106*, 23,073–23,096.

Blond, N., K. F. Boersma, H. J. Eskes, R. J. van der A, M. Van Roozendael, I. De Smedt, G. Bergametti, and R. Vautard (2007), Intercomparison of SCIAMAHCY nitrogen dioxide observations, in situ measurements and air quality modeling results over Western Europe, *J. Geophys. Res.*, *112*, D10311, doi:10.1029/2006JD007277.

Boersma, K. F., H. J. Eskes, and E. J. Brinksma (2004), Error analysis for tropospheric NO_2 retrieval from space, *J. Geophys. Res.*, *109*, D04311, doi:10.1029/2003JD003962.

Boersma, K. F., H. J. Eskes, E. W. Meijer, and H. M. Kelder (2005), Estimates of lightning NO_x production from GOME satellite observations, *Atmos. Chem. Phys.*, *5*, 2311–2331.

Boersma, K. F., et al. (2007), Near-real time retrieval of tropospheric NO_2 from OMI, *Atmos. Chem. Phys.*, *112*, 2103–2118.

Boersma, K. F., D. J. Jacob, H. J. Eskes, R. W. Pinder, J. Wang, and R. J. van der A (2008a), Intercomparison of SCIAMACHY and OMI tropospheric NO_2 columns: Observing the diurnal evolution of chemistry and emissions from space, *J. Geophys. Res.*, *113*, D16S26, doi:10.1029/2007JD008816.

Boersma, K. F., et al. (2008b), Validation of OMI tropospheric NO_2 observations during INTEX-B and application to constrain NO_x emissions over the eastern United States and Mexico, *Atmos. Environ.*, *42*, 4480–4497.

Boersma, K. F., D. J. Jacob, M. Trainic, Y. Rudich, I. DeSmedt, R. Dirksen, and H. J. Eskes (2009), Validation of urban NO_2 concentrations and their diurnal and seasonal variations observed from the SCIAMACHY and OMI sensors using in situ surface measurements in Israeli cities, *Atmos. Chem. Phys.*, *9*, 3867–3879.

Brinksma, E., et al. (2008), The 2005 and 2006 DANDELIONS NO_2 and Aerosol Intercomparison Campaigns, *J. Geophys. Res.*, *113*, D16S46, doi:10.1029/2007JD008808.

Bucsela, E. J., E. A. Celarier, M. O. Wenig, J. F. Gleason, J. P. Veefkind, K. F. Boersma, and E. J. Brinksma (2006), Algorithm for NO_2 vertical column retrieval from the Ozone Monitoring Instrument, *IEEE Trans. Geosci. Remote Sens.*, *44*, 1245–1258.

Bucsela, E. J., et al. (2008), Comparison of NO_2 in situ aircraft measurements with data from the Ozone Monitoring Instrument, *J. Geophys. Res.*, *113*, D16S31, doi:10.1029/2007JD008838.

Burnett, R. T., D. Steib, J. R. Brook, S. Cakmak, R. Dales, M. Raizenne, R. Vincent, and T. Dann (2004), The short-term effects of nitrogen dioxide on mortality in Canadian cities, *Arch. Environ. Health*, *59*, 228–237.

Celarier, E. A., et al. (2008), Validation of ozone monitoring instrument nitrogen dioxide columns, *J. Geophys. Res.*, *113*, D15S15, doi:10.1029/2007JD008908.

Choi, Y., Y. H. Wang, T. Zeng, R. V. Martin, T. P. Kurosu, and K. Chance (2005), Evidence of lightning NO_x and convective transport of pollutants in satellite observations over North America, *Geophys. Res. Lett.*, *32*, L02805, doi:10.1029/2004GL021436.

Demerjian, K. L. (2000), A review of national monitoring networks in North America, *Atmos. Environ.*, *34*, 1861–1884.

Dentener, F., W. Peter, M. Krol, M. van Weele, P. Bergamaschi, and J. Lelieveld (2003), Interannual variability and trend of OH and the lifetime of CH_4: 1979–1993 global chemical transport model calculations, *J. Geophys. Res.*, *108*(D15), 4442, doi:10.1029/2002JD002916.

Dentener, F. J., and P. J. Crutzen (1993), Reaction of N_2O_5 on tropospheric aerosols: Impact on the global distributions of NO_x, O_3, and OH, *J. Geophys. Res.*, *98*, 7149–7162.

Dobber, M. R., et al. (2008), Validation of ozone monitoring instrument level 1b data products, *J. Geophys. Res.*, *113*, D15S06, doi:10.1029/2007JD008665.

Dommen, J., A. S. H. Prèvôt, A. M. Hering, T. Staffelbach, G. L. Kok, and R. D. Schillawski (1999), Photochemical production and ageing of an urban air mass, *J. Geophys. Res.*, *104*, 5493–5509.

Duncan, B. N., R. V. Martin, A. C. Staudt, R. Yevich, and J. A. Logan (2003), Interannual and seasonal variability of biomass burning emissions constrained by satellite observations, *J. Geophys. Res.*, *108*(D2), 4100, doi:10.1029/2002JD002378.

Dunlea, E. J., et al. (2007), Evaluation of nitrogen dioxide chemiluminescence monitors in a polluted urban environment, *Atmos. Chem. Phys.*, *7*, 2691–2704.

Environmental Protection Agency (EPA) (1975), Technical assistance document for the chemiluminescence measurement of nitrogen dioxide, *Tech. Rep.*, Environmental Monitoring and Support Laboratory, U.S. Environmental Protection Agency, Research Triangle Park, N.C. 27711, EPA-600/4-75-003.

Environmental Protection Agency (EPA) (2008), Integrated Science Assessment for Oxides of Nitrogen: Health Criteria (First External Review Draft), *Tech. Rep.*, U.S. Environmental Protection Agency, Research Triangle Park, NC 27711, EPA/600/R-07/093.

Environmental Protection Agency (EPA) (2009), Primary national ambient air quality standard for nitrogen dioxide, *Tech. Rep.*, Environmental Protection Agency, Federal Register, Vol. 74, No. 134.

Eskes, H. J., and K. F. Boersma (2003), Averaging kernels for DOAS total-column satellite retrievals, *Atmos. Chem. Phys.*, *3*, 1285–1291.

Evans, M. J., and D. J. Jacob (2005), Impact of new laboratory studies of N_2O_5 hydrolysis on global model budgets of tropospheric nitrogen oxides, ozone and OH, *Geophys. Res. Lett.*, *32*, L09813, doi:10.1029/2005GL022469.

Fehsenfeld, F. C., et al. (1990), Intercomparison of NO_2 measurement techniques, *J. Geophys. Res.*, *95*, 3579–3597.

Frost, G. J., et al. (2006), Effects of changing power plant NO_x emissions on ozone in the eastern United States: Proof of concept, *J. Geophys. Res.*, *111*, D12306, doi:10.1029/2005JD006354.

Grosjean, D., and J. Harrison (1985), Response of chemiluminescence NO_x analyzers and ultraviolet ozone analyzers to organic air pollutants, *Environ. Sci. Technol.*, *19*, 862–865.

Hains, J., et al. (2010), Testing and improving OMI DOMINO tropospheric NO_2 using observations from the DANDELIONS and INTEX-B validation campaigns, *J. Geophys. Res.*, doi:10.1029/2009JD012399, in press.

Hansen, D. A., E. S. Edgerton, B. E. Hartsell, J. J. Jansen, N. Kandasamy, G. M. Hidy, and C. L. Blanchard (2003), The southeastern aerosol research and characterization study. Part 1: Overview, *J. Air Waste Manage. Assoc.*, *53*, 1460–1471.

Heland, J., H. Schlager, A. Richter, and J. P. Burrows (2002), First comparison of tropospheric NO_2 column densities retrieved from GOME measurements and in situ aircraft profile measurements, *Geophys. Res. Lett.*, *29*(20), 1983, doi:10.1029/2002GL015528.

Herman, J. R., and E. A. Celarier (1997), Earth surface reflectivity climatology at 340 nm to 380 nm from TOMS data, *J. Geophys. Res.*, *102*, 28,003–28,011, doi:10.1029/97JD02074.

Hudman, R. C., et al. (2007), Surface and lightning sources of nitrogen oxides over the United States: Magnitudes, chemical evolution, and outflow, *J. Geophys. Res.*, *112*, D12S05, doi:10.1029/2006JD007912.

Hudman, R. C., L. T. Murray, D. J. Jacob, S. Turquety, S. Wu, D. B. Millet, M. Avery, A. H. Goldstein, and J. Holloway (2009), North American influence on tropospheric ozone and the effects of recent emission reductions: Constraints from ICARTT observations, *J. Geophys. Res.*, *114*, D07302, doi:10.1029/2008JD010126.

Huijnen, V., et al. (2009), Comparison of OMI NO_2 tropospheric columns with an ensemble of global and European air quality models, *Atmos. Chem. Phys. Discuss.*, *9*, 22,271–22,330.

Ionov, D. V., Y. M. Timofeyev, V. P. Sinyakov, V. K. Semenov, F. Goutail, J. P. Pommereau, E. J. Bucsela, E. A. Celarier, and M. Kroon (2008), Ground-based validation of EOS-Aura OMI NO_2 vertical column data in the midlatitude mountain ranges of Tien Shan (Kyrgyzstan) and Alps (France), *J. Geophys. Res.*, *113*, D15S08, doi:10.1029/2007JD008659.

Irie, H., Y. Kanaya, H. Akimoto, H. Tanimoto, F. G. Z. J.Wang, and E. J. Bucsela (2008), Validation of OMI tropospheric NO_2 column data using MAX-DOAS measurements deep inside the North China Plain in June 2006, *Atmos. Chem. Phys. Disc.*, *8*, 8243–8271.

Jacob, D. J. (2000), Heterogeneous chemistry and tropospheric ozone, *Atmos. Environ.*, *34*, 2131–2159.

Jaeglé, L., et al. (2004), Satellite mapping of rain-induced nitric oxide emissions from soils, *J. Geophys. Res.*, *109*, D21310, doi:10.1029/2004JD004787.

Jaeglé, L., L. Steinberger, R. V. Martin, and K. Chance (2005), Global partitioning of NO_x sources using satellite observations: Relative roles of fossil fuel combustion, biomass burning and soil emissions, *Faraday Discus.*, *130*, 407–423, doi:10.1039/b502128f.

Kaynak, B., Y. Hu, R. V. Martin, A. G. Russell, and C. Sioris (2008), Comparison of weekly cycle of NO_2 satellite retrievals and NO_x emission inventories for the continental U.S., *J. Geophys. Res.*, *114*, D05302, doi:10.1029/2008JD010714.

Kley, D., and M. McFarland (1980), Chemiluminescence detector for NO and NO_2, *Atmos. Tech.*, *12*, 63–69.

Koelemeijer, A. R. B., J. F. de Haan, and P. Stammes (2003), A database of spectral surface reflectivity in the range 335–772 nm derived from 5.5 years of GOME observations, *J. Geophys. Res.*, *108*(D2), 4070, doi:10.1029/2002JD002429.

Kramer, L. J., R. J. Leigh, J. J. Remedios, and P. S. Monks (2008), Comparison of OMI and ground-based in situ and MAX-DOAS measurements of tropospheric nitrogen dioxide in an urban area, *J. Geophys. Res.*, *113*, D16S39, doi:10.1029/2007JD009168.

Kuhns, H., E. M. Knipping, and J. M. Vokovich (2005), Development of a United States-Mexico emissions inventory for the Big Bend Regional Aerosol and Visibility Observational (BRAVO) study, *J. Air Waste Manage. Assoc.*, *55*, 677–692.

Kunhikrishnan, T., and M. G. Lawrence (2004), Sensitivity of NO_x over the Indian Ocean to emissions from the surrounding continents and nonlinearities in atmospheric chemistry responses, *Geophys. Res. Lett.*, *31*, L15109, doi:10.1029/2004GL020210.

Lambert, J. C., et al. (2004), Geophysical validation of SCIAMACHY NO_2 vertical columns: Overview of early 2004, in *Proceedings of the Second Workshop on the Atmospheric Chemistry Validation of ENVISAT (ACVE-2)*, pp. 6.1–6.13, ESA-ESRIN, Frascati, Italy, 3–7 May.

Lamsal, L. N., R. V. Martin, A. van Donkelaar, M. Steinbacher, E. A. Celarier, E. Bucsela, E. J. Dunlea, and J. P. Pinto (2008), Ground-level nitrogen dioxide concentrations inferred from the satellite-borne Ozone Monitoring Instrument, *J. Geophys. Res.*, *113*, D16308, doi:10.1029/2007JD009235.

Lauer, A., M. Dameris, A. Richter, and J. P. Burrows (2002), Tropospheric NO_2 columns: A comparison between model and retrieved data from GOME measurements, *Atmos. Chem. Phys.*, *2*, 67–78.

Leue, C., M. Wenig, T. Wagner, O. Klimm, U. Platt, and B. Jähne (2001), Quantitative analysis of NO_2 emissions from Global Ozone Monitoring Experiment satellite image sequences, *J. Geophys. Res.*, *106*, 5493–5505.

Levelt, P. F., E. Hilsenrath, G. W. Leppelmeier, G. B. J. van den Oord, P. K. Bhartia, J. Tamminen, J. F. de Haan, and J. P. Veefkind (2006a), Science objective of the Ozone Monitoring Instrument, *IEEE Trans. Geosci. Remote Sens.*, *44*, 1199–1208.

Levelt, P. F., G. H. J. van den Oord, M. R. Dobber, A. Malkki, H. Visser, J. de Vries, P. Stammes, J. O. V. Lundell, and H. Saari (2006b), The Ozone Monitoring Instrument, *IEEE Trans. Geosci. Remote Sens.*, *44*, 1093–1101.

Martin, R. V., et al. (2002), An improved retrieval of tropospheric nitrogen dioxide from GOME, *J. Geophys. Res.*, *107*(D20), 4437, doi:10.1029/2001JD001027.

Martin, R. V., D. J. Jacob, K. Chance, T. P. Kurosu, P. I. Perner, and M. J. Evans (2003a), Global inventory of nitrogen oxide emission constrained by space-based observations of NO_2 columns, *J. Geophys. Res.*, *108*(D17), 4537, doi:10.1029/2003JD003453.

Martin, R. V., D. J. Jacob, R. M. Yantosca, M. Chin, and P. Ginoux (2003b), Global and regional decreases in tropospheric oxidants from photochemical effects of aerosols, *J. Geophys. Res.*, *108*(D3), 4097, doi:10.1029/2002JD002622.

Martin, R. V., et al. (2004), Evaluation of GOME satellite measurements of tropospheric NO_2 and HCHO using regional data from aircraft campaigns in the southeastern United States, *J. Geophys. Res.*, *109*, D24307, doi:10.1029/2004JD004869.

Martin, R. V., et al. (2006), Evaluation of space-based constraints on global nitrogen oxide emissions with regional aircraft measurements over and downwind of eastern North America, *J. Geophys. Res.*, *111*, D15308, doi:10.1029/2005JD006680.

Martin, R. V., B. Sauvage, I. Folkins, C. E. Sioris, C. Boone, P. Bernath, and J. R. Ziemke (2007), Space-based constraints on the production of nitric oxide by lightning, *J. Geophys. Res.*, *112*, D09309, doi:10.1029/2006JD007831.

Morris, R. E., B. Koo, B. Wang, G. Stella, D. McNally, C. Loomis, C. J. Chien, and G. Tonnesen (2007), Technical support document for VISTAS emissions and air quality modeling to support regional haze State Implementation Plans, *Tech. Rep.*, VISTAS Technical Coordinator, http://pah.cert.ucr.edu/vistas/vistas2/reports/TSD/.

Müller, J., and T. Stavrakou (2005), Inversion of CO and NO_2 emissions using the adjoint of the IMAGES model, *Atmos. Chem. Phys.*, *5*, 1157–1186.

Napelenok, S. L., R. W. Pinder, A. B. Gilliland, and R. V. Martin (2008), A method for evaluating spatially-resolved NO_x emissions using Kalman filter inversion, direct sensitivities, and space-based NO_2 observations, *Atmos. Chem. Phys.*, *8*, 5603–5614.

NARSTO (2005), Improving emission inventories for effective air quality management across North America: A NARSTO Assessment, *Tech. Rep.*, NARSTO, http://www.narsto.org/, NARSTO-05-001.

Neuman, J. A., L. G. Huey, T. B. Ryerson, and D. W. Fahey (1999), Study of inlet materials for sampling atmospheric nitric acid, *Environ. Sci. Technol.*, *33*, 1133–1136.

Nunnermacker, L. J., et al. (1998), Characterization of the Nashville urban plume on July 3 and July 18, 1995, *J. Geophys. Res.*, *103*, 28,129–28,148.

Nunnermacker, L. J., L. I. Kleinman, D. Imre, P. H. Daum, Y. N. Lee, J. H. Lee, S. R. Springston, and L. Newman (2000), NO_y lifetimes and O_3 production efficiencies in urban and power plant plumes: Analysis of field data, *J. Geophys. Res.*, *105*, 9165–9176.

Olivier, J. G. J., J. J. M. Berdowski, J. A. H. W. Peters, J. Bakker, A. J. H. Visschedijk, and J. P. J. Bloos (2001), Applications of EDGAR, including a description of EDGAR 3.2: Reference database with trend data for

1970–1995, *Tech. Rep.*, RIVM Bilthovan, RIVM report, 773301001/NRP report 4.

Ordóñez, C., A. Richter, M. Steinbacher, C. Zellweger, H. Nüß, and J. P. Burrows (2006), Comparison of 7 years of satellite-borne and ground-based tropospheric NO_2 measurements around Milan, Italy, *J. Geophys. Res.*, *111*, D05310, doi:10.1029/2005JD006305.

Palmer, P. I., D. J. Jacob, A. M. Fiore, R. V. Martin, K. Chance, and T. P. Kurosu (2003), Mapping isoprene emissions over North America using formaldehyde column observations from space, *J. Geophys. Res.*, *108*(D6), 4180, doi:10.1029/2002JD002153.

Parrish, D. D., et al. (1990), Systematic variations in the concentration of NO_x (NO plus NO_2) at Niwot Ridge, Colorado, *J. Geophys. Res.*, *95*, 1817–1836.

Pickering, K. E., Y. S. Wang, W. K. Tao, C. Price, and J. F. Muller (1998), Vertical distribution of lightning NO_x for use in regional and global chemical transport models, *J. Geophys. Res.*, *103*, 31,203–31,216.

Price, C., and D. Rind (1992), A simple lightning parameterization for calculating global lightning distribution, *J. Geophys. Res.*, *97*, 9919–9933.

Richter, A., V. Eyring, J. P. Burrows, H. Bovensmann, A. Lauer, B. Sierk, and P. J. Crutzen (2004), Satellite measurements of NO_2 from international shipping emissions, *Geophys. Res. Lett.*, *31*, L23110, doi:10.1029/2004GL020822.

Richter, A., J. P. Burrows, H. Nüß, C. Granier, and U. Niemeier (2005), Increase in tropospheric nitrogen dioxide levels over China observed from space, *Nature*, *437*, 129–132.

Ryerson, T. B., E. J. Williams, and F. C. Fehsenfeld (2000), An efficient photolysis system for fast-response NO_2 measurements, *J. Geophys. Res.*, *105*, 26,447–26,461.

Ryerson, T. B., et al. (2003), Effect of petrochemical industrial emissions of reactive alkenes and NO_x on tropospheric ozone formation in Houston, Texas, *J. Geophys. Res.*, *108*(D8), 4249, doi:10.1029/2002JD003070.

Samoli, E., et al. (2006), Short term effects of nitrogen dioxide and mortality: An analysis within the APHEA project, *Eur. Respir. J.*, *27*, 1129–1137.

Sauvage, B., R. V. Martin, A. van Donkelaar, X. Liu, K. Chance, L. Jaeglé, P. I. Palmer, S. Wu, and T. M. Fu (2007), Remote sensed and in situ constraints on processes affecting tropical tropospheric ozone, *Atmos. Chem. Phys.*, *7*, 815–838.

Schaub, D., D. Brunner, K. F. Boersma, J. Keller, D. Folini, B. Buchmann, H. Berresheim, and J. Staehelin (2007), SCIAMACHY tropospheric NO_2 over Switzerland: Estimates of NO_2 lifetimes and impact of the complex Alpine topography on the retrieval, *Atmos. Chem. Phys.*, *7*, 5971–5987.

Sillman, S. (2000), Ozone production efficiency and loss of NO_x in power plant plumes: Photochemical model and interpretation of measurements in Tennesse, *J. Geophys. Res.*, *105*, 9189–9202.

Singh, H. B., et al. (2007), Reactive nitrogen distribution and partitioning in the North American troposphere and lowermost stratosphere, *J. Geophys. Res.*, *112*, D12S04, doi:10.1029/2006JD007664.

Spicer, C. W. (1982), Nitrogen dioxide reactions in the urban plume of Boston, *Science*, *215*, 1095–1097.

Stammes, P. (2001), Spectral radiance modelling in the UV-Visible range, in *IRS 2000: Current problems in Atmospheric Radiation*, edited by W. L. Smith and Y. M. Timofeyev, pp. 385–388, A. Deepak Publ., Hampton, Va.

Steib, D., S. Judek, and R. T. Brunett (2003), Meta-analysis of time-series studies of air pollution and mortality: Update in relation to the use of generalized additive models, *J. Air Waste Manage. Assoc.*, *53*, 258–261.

Steinbacher, M., C. Zellweger, B. Schwarzenbach, S. Bugmann, B. Buchmann, C. Ordòñez, A. S. H. Prèvôt, and C. Hueglin (2007), Nitrogen oxides measurements at rural sites in Switzerland: Bias of conventional measurement techniques, *J. Geophys. Res.*, *112*, D11307, doi:10.1029/2006JD007971.

Streets, D. G., et al. (2003), An inventory of gaseous and primary aerosol emissions in Asia in the year 2000, *J. Geophys. Res.*, *108*(D21), 8809, doi:10.1029/2002JD003093.

Streets, D. G., Q. Zhang, L. Wang, K. He, J. Hao, Y. Wu, Y. Tang, and G. R. Carmichael (2006), Revisiting China's CO emissions after the Transport and Chemical Evolution over the Pacific (TRACE-P) mission: Synthesis of inventories, atmospheric modeling, and observations, *J. Geophys. Res.*, *111*, D14306, doi:10.1029/2006JD007118.

Toenges-Schüller, N., et al. (2006), Global distribution pattern of anthropogenic nitrogen oxide emissions: Correlation analysis of satellite measurements and model calculations, *J. Geophys. Res.*, *111*, D05312, doi:10.1029/2005JD006068.

van der A, R. J., D. H. M. Peters, H. Eskes, K. F. Boersma, M. Van Roozendael, I. De Smedt, and H. M. Kelder (2006), Detection of the trend and seasonal variation in tropospheric NO_2 over China, *J. Geophys. Res.*, *111*, D12317, doi:10.1029/2005JD006594.

van der A, R. J., H. J. Eskes, K. F. Boersma, T. P. C. van Noije, M. Van Roozendael, I. De Smedt, D. H. M. Peters, J. J. P. Kuenen, and E. W. Meijer (2008), Identification of NO_2 sources and their trends from space using seasonal variability analyses, *J. Geophys. Res.*, *113*, D04302, doi:10.1029/2007JD009021.

van Donkelaar, A., et al. (2008), Analysis of aircraft and satellite measurements from the Intercontinental Chemical Transport Experiment (INTEX-B) to quantify long-range transport of East Asian sulfur to Canada, *Atmos. Chem. Phys.*, *8*, 2999–3014.

van Noije, T. P. C., et al. (2006), Multi-model ensemble simulations of tropospheric NO_2 compared with GOME retrievals for the year 2000, *Atmos. Chem. Phys.*, *6*, 2943–2979.

Velders, G. J. M., C. Granier, R. W. Portmann, K. Pfeilsticker, M. Wenig, T. Wagner, U. Platt, A. Richter, and J. P. Burrows (2001), Global tropospheric NO_2 distributions: Comparing 3-D model calculations with GOME measurements, *J. Geophys. Res.*, *106*, 12,643–12,660.

Vestreng, V., K. Mareckova, S. Kakareka, A. Malchykhina, and T. Kukharchyk (2007), Inventory review 2007. Emission data reported to LRTAP and NEC Directive. Stage 1 and 2 review, review of gridded data and review of PM inventories in Belarus, Republic of Moldova, and Russian Federation and Ukraine, *Tech. Rep.*, EMEP technical report 1/2007, Oslo, Norway, ISSN 1504-6079.

Vestreng, V., L. Ntziachristos, A. Semb, S. Reis, I. S. A. Isaksen, and L. Terrasón (2009), Evolution of NO_x emissions in Europe with focus on road transport control measures, *Atmos. Chem. Phys.*, *9*, 1503–1520.

Wang, Y., D. J. Jacob, and J. A. Logan (1998), Global simulation of tropospheric O_3-NO_x-hydrocarbon chemistry, 1. Model formulation, *J. Geophys. Res.*, *103*, 10,713–10,726.

Wang, Y. X., M. B. McElroy, R. V. Martin, D. G. Streets, Q. Zhang, and T.-M. Fu (2007), Seasonal variability of NO_x emissions over east China constrained by satellite observations: Implications for combustion and microbial sources, *J. Geophys. Res.*, *112*, D06301, doi:10.1029/2006JD007538.

Wenig, M. O., A. M. Cede, E. J. Bucsela, E. A. Celarier, F. K. Boersma, J. P. Veefkind, E. J. Brinksma, J. F. Gleason, and J. R. Herman (2008), Validation of OMI tropospheric NO_2 column densities using direct-Sun mode Brewer measurements at NASA Goddard Space Flight Center, *J. Geophys. Res.*, *113*, D16S45, doi:10.1029/2007JD008988.

Winer, A. M., J. W. Peters, J. P. Smith, and J. N. Pitts Jr. (1974), Response of commercial chemiluminescent NO-NO_2 analyzers to other nitrogen containing compounds, *Environ. Sci. Technol.*, *8*, 1118–1121.

Yienger, J. J., and H. Levy (1995), Empirical model of global soil biogenic NO_x emissions, *J. Geophys. Res.*, *100*, 11,447–11,464.

Zellweger, C., M. Ammann, B. Buchmann, P. Hofer, M. Lugauer, R. Rüttimann, N. Streit, E. Weingartner, and U. Baltensperger (2000), Summertime NO_y speciation at the Jungfraujoch, 3580 m above sea level, Switzerland, *J. Geophys. Res.*, *105*, 6655–6667.

Zhang, L., et al. (2008), Transpacific transport of ozone pollution and the effect of recent Asian emission increases on air quality in North America: An integrated analysis using satellite, aircraft, ozonesonde, and surface observations, *Atmos. Chem. Phys.*, *8*, 6117–6136.

Zhang, Q., et al. (2007), NO_x emission trends for China, 1995–2004: The view from the ground and the view from space, *J. Geophys. Res.*, *112*, D22306, doi:10.1029/2007JD008684.

Zhang, Q., et al. (2009), Asian emissions in 2006 for the NASA INTEX-B mission, *Atmos. Chem. Phys. Disc.*, *9*, 4081–4139.

Zhao, C., and Y. Wang (2009), Assimilation inversion of NO_2 emissions over east Asia using OMI NO_2 column measurements, *Geophys. Res. Lett.*, *36*, L06805, doi:10.1029/2008GL037123.

Zhou, Y., D. Brunner, K. F. Boersma, R. Dirksen, and P. Wang (2009), An improved tropospheric NO_2 retrieval for OMI observations in the vicinity of mountainous terrain, *Atmos. Meas. Tech.*, *2*, 401–416.

K. F. Boersma and R. Dirksen, Climate Observations Department, Royal Netherlands Meteorological Institute, Wilhelminalaan 10, NL-3732 GK De Bilt, Netherlands.

E. J. Bucsela, SRI International, 333 Ravenswood Ave., Menlo Park, CA 94025-3493, USA.

E. A. Celarier, Goddard Earth Sciences and Technology Center, University of Maryland Baltimore County, Baltimore, MD 21228, USA.

L. N. Lamsal, R. V. Martin, and A. van Donkelaar, Department of Physics and Atmospheric Science, Dalhousie University Halifax, James Dunn Building, Halifax, NS B3H 3J5, Canada. (lok.lamsal@fizz.phys.dal.ca)

C. Luo and Y. Wang, School of Earth and Atmospheric Sciences, Georgia Institute of Technology, Atlanta, GA 30332, USA.